

Reconfigurable Switched-Capacitor Converter for Maximum Power Point Tracking of PV System

Yuen-Haw Chang, Chin-Ling Chen and Tzu-Chi Lin

Abstract—A reconfigurable switched-capacitor converter (RSCC) is proposed by combining averaged perturb and observe (APO) algorithm for the maximum power point tracking (MPPT) of the photovoltaic (PV) module system. In the RSCC, there are totally 7 modes operating for the different topologies to perform the various serial/parallel connections of buffer capacitors. Thus, we can obtain the different input equivalent resistance of SC bank to manipulate so as to search and track the maximum power point (MPP) of the power module. Here, the APO-based controller is presented and designed for making a decision according to the terminal voltage and current of PV module to increase or decrease the “running” number of buffer capacitors for harvesting the energy as more as possible. Finally, some cases (steady-state/dynamic responses) are discussed and simulated via OrCAD Pspice, and the results are illustrated to show the efficacy of the proposed scheme.

Index Terms—maximum power point tracking (MPPT), switched-capacitor (SC), photovoltaic (PV), averaged perturb and observe (APO).

I. INTRODUCTION

In recent years, due to the limitation of gas fuel on earth, people must seek for alternative kinds of green energy, such as water energy, solar energy,...etc. Among them, the solar energy is now widely used because it is a clean, maintenance-free, safe, and abundant resource of nature. But, there are still some problems: (i) The install cost of solar cells is higher. (ii) The conversion efficiency of solar cells is lower. (iii) It is not a constant long-term energy because the sunlight intensity and temperature level of solar cells change anytime [1]. A PV module, possessed of several solar cells, has the unique characteristic of current versus voltage (I - V) [1]-[4]. Further, plus considering the environmental factors (sunlight intensity, temperature), it leads to increase the complexity of MPPT. To overcome this problem, many MPPT algorithms have been presented [1], [2], and one of well-known algorithms is perturbation and observation algorithm (P&O algorithm) [3]. This P&O algorithm has the advantages of low cost and simple circuit. However, the steady-state oscillations often appear in P&O methods. Thus, it makes some power loss and slower tracking response.

Manuscript received December 12, 2013. This work is supported in part by the National Science Council of Taiwan, R.O.C., under Grant NSC 102-2221-E-324-030.

Yuen-Haw Chang, Chin-Ling Chen and Tzu-Chi Lin are with the Department and Graduate Institute of Computer Science and Information Engineering, Chaoyang University of Technology, Taichung, Taiwan, R.O.C. Post: 413. (e-mail: cyhfvc@cyut.edu.tw, clc@mail.cyut.edu.tw, s10127631@gm.cyut.edu.tw).

The SC power converter based on structure of charge pump is one of the good solutions to low power and step-up/down DC-DC conversion because it has only semiconductor switches and capacitors. Unlike traditional converters, SC converter needs no magnetic element, so it has light weight, small volume and low EMI. Now, various SC types have been suggested and the well-known topologies are described as follow. In 1976, Dickson charge pumping was proposed based on a diode-chain structure via pumping capacitors [5]. It provides voltage gain proportional to the stage number of pumping capacitor, and the detailed dynamic model and efficiency analysis were discussed [6]. In 1993, Ioinovici *et al.* suggested a voltage-mode SC with two symmetrical capacitor cells working complementarily [7]. In 1997, Zhu and Ioinovici performed a comprehensive steady-state analysis of SC [8]. In 2009, Tan *et al.* proposed a low-EMI SC by interleaving control [9]. In 2011, Chang proposed an integrated SC step-up/down DC-DC/DC-AC converter/inverter [10], [11]. Recently, Chang *et al.* suggested a gain/efficiency-improved SC scheme by adapting the stage number [12]. In 2012, Peter and Agarwal proposed a reconfigurable SC DC-DC converter for MPPT of a PV source [13]. In this paper, we try to make an attempt on the development of RSCC combined with a modified averaged P&O (APO) algorithm for realigning MPPT of the PV module.

II. CONFIGURATION

Fig.1 shows the overall configuration of RSCC system. In this figure, the system includes three parts: (i) PV module, (ii) RSCC circuit, and (iii) APO-based controller. Let's consider these parts as follows.

A. PV module

In general, the equivalent models of solar cell have three types as in Fig. 2. Fig. 2(a) shows an ideal model just with one current source I_{rated} and diode. Fig. 2(b) has an extra small resistor to simulate the line loss. Fig. 2(c) has a big internal resistor to realize the solar cell's power loss. In this paper, we choose the model of Fig. 2(b) for the simulation later. Each solar cell has its own characteristic I - V curve. The terminal current I_{pv} and voltage V_{pv} change with sunlight intensity and temperature level, so does output power of PV module, where I_{pv} and V_{pv} are the total current and voltage of PV module, respectively. In Fig. 3, the dash line shows the I - V curves of a solar cell, and the bold line represents the P - V curve, where V_{oc} is the open-circuit voltage of PV module and I_{sc} is the short-circuit current. Of course, if $I_{pv}=I_{sc}$ or $V_{pv}=V_{oc}$, then the output power of PV module will be zero. Thus, we can track the maximum power point (MPP) of solar cell by regulating the operating

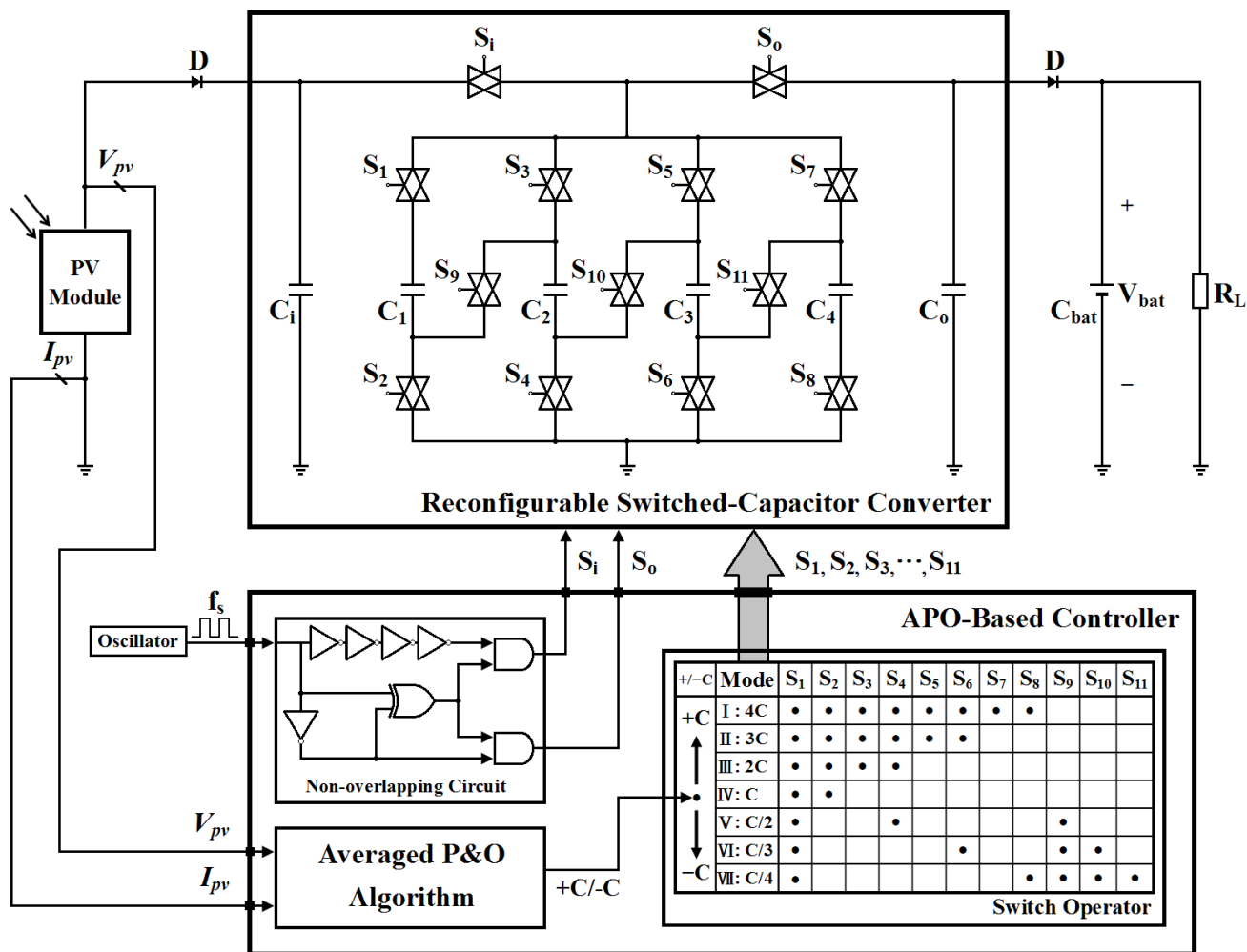


Fig. 1. Configuration of RSCC for MPPT.

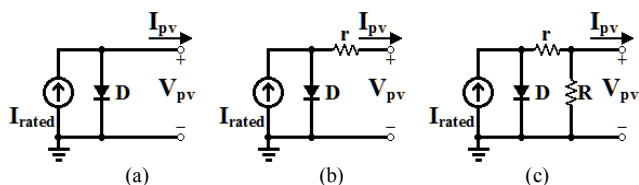


Fig. 2. Equivalent models of solar cell.

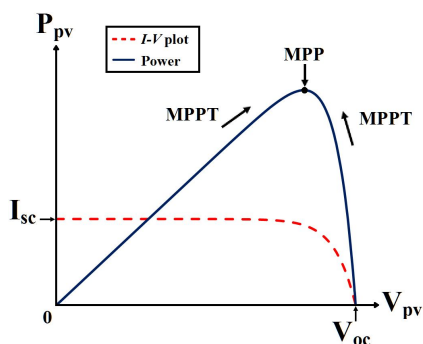


Fig. 3. Characteristic of I - V and P - V curves.

voltage of V_{pv} .

B. RSCC circuit

The RSCC circuit as in the upper half of Fig. 1 is located between the PV module and the battery load. For

more details, it includes 4 buffer capacitors (C_1 , C_2 , C_3 and C_4), one input capacitor C_i , one output capacitor C_o and 13 switches (S_i , S_o , S_1 - S_{11}), where each buffer capacitor has the same capacitance C ($C_1=C_2=C_3=C_4=C$). The detailed operation of RSCC will be discussed in the section III.

C. APO-based controller

The APO-based controller is shown in the lower half of Fig. 1, and it contains three parts: (i) averaged P&O (APO) algorithm, (ii) non-overlapping circuit, and (iii) switch operator. And this kind of APO-based controller can be easily made by digital microcontroller unit (MCU). The detailed operation of APO-based controller will be discussed in the section IV.

III. OPERATION OF RSCC

In the RSCC, there are totally 7 modes (mode I, II, III, IV, V, VI, VII) operating for the different topologies. These topologies can perform the various serial/parallel connections of buffer capacitors. Thus, the total input capacitance from the view of PV module will be regulated flexibly so that the goal of MPPT can be achieved by switching these modes. For each mode, there are cyclically two phases (Phase I and II) operating in one switching cycle T_s ($T_s=1/f_s$, f_s is the switching frequency). Here, Phase I/II represents that the buffer capacitors are running

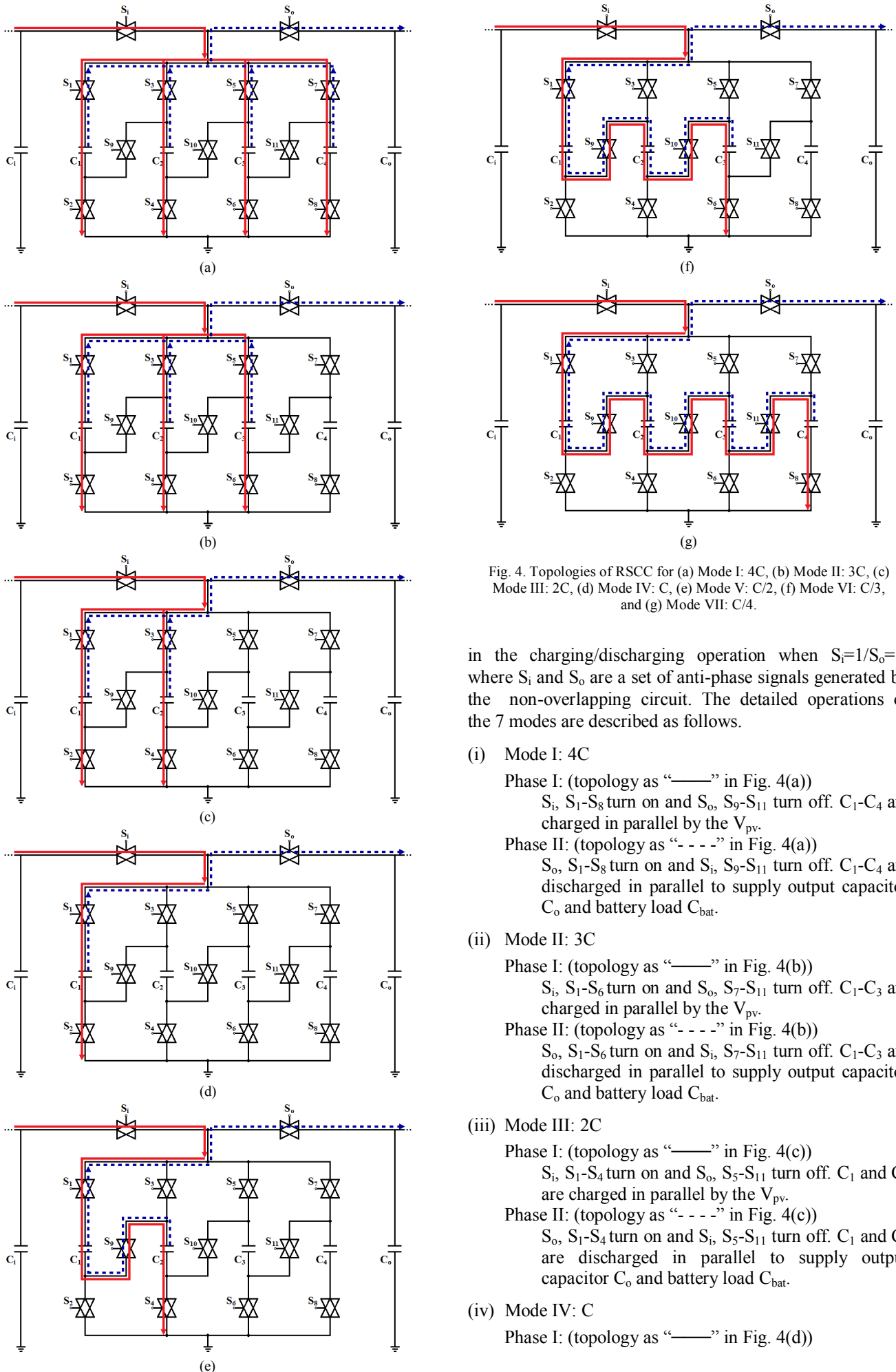


Fig. 4. Topologies of RSCC for (a) Mode I: 4C, (b) Mode II: 3C, (c) Mode III: 2C, (d) Mode IV: C, (e) Mode V: C/2, (f) Mode VI: C/3, and (g) Mode VII: C/4.

in the charging/discharging operation when $S_i=1/S_o=1$, where S_i and S_o are a set of anti-phase signals generated by the non-overlapping circuit. The detailed operations of the 7 modes are described as follows.

(i) Mode I: 4C

Phase I: (topology as “——” in Fig. 4(a))

S_i, S_1-S_8 turn on and S_o, S_9-S_{11} turn off. C_1-C_4 are charged in parallel by the V_{pv} .

Phase II: (topology as “- - - -” in Fig. 4(a))

S_o, S_1-S_8 turn on and S_i, S_9-S_{11} turn off. C_1-C_4 are discharged in parallel to supply output capacitor C_o and battery load C_{bat} .

(ii) Mode II: 3C

Phase I: (topology as “——” in Fig. 4(b))

S_i, S_1-S_6 turn on and S_o, S_7-S_{11} turn off. C_1-C_3 are charged in parallel by the V_{pv} .

Phase II: (topology as “- - - -” in Fig. 4(b))

S_o, S_1-S_6 turn on and S_i, S_7-S_{11} turn off. C_1-C_3 are discharged in parallel to supply output capacitor C_o and battery load C_{bat} .

(iii) Mode III: 2C

Phase I: (topology as “——” in Fig. 4(c))

S_i, S_1-S_4 turn on and S_o, S_5-S_{11} turn off. C_1 and C_2 are charged in parallel by the V_{pv} .

Phase II: (topology as “- - - -” in Fig. 4(c))

S_o, S_1-S_4 turn on and S_i, S_5-S_{11} turn off. C_1 and C_2 are discharged in parallel to supply output capacitor C_o and battery load C_{bat} .

(iv) Mode IV: C

Phase I: (topology as “——” in Fig. 4(d))

S_i , S_1 - S_2 turn on and S_o , S_3 - S_{11} turn off. C_1 is charged by the V_{pv} .

Phase II: (topology as “- - -” in Fig. 4(d))

S_o , S_1 - S_2 turn on and S_i , S_3 - S_{11} turn off. C_1 is discharged to supply output capacitor C_o and battery load C_{bat} .

(v) Mode V: C/2

Phase I: (topology as “——” in Fig. 4(e))

S_i , S_1 , S_4 , S_9 turn on and S_o , S_2 , S_3 , S_5 - S_8 , S_{10} , S_{11} turn off. C_1 and C_2 are charged in series by the V_{pv} .

Phase II: (topology as “- - -” in Fig. 4(e))

S_o , S_1 , S_4 , S_9 turn on and S_i , S_2 , S_3 , S_5 - S_8 , S_{10} , S_{11} turn off. C_1 and C_2 are discharged in series to supply output capacitor C_o and battery load C_{bat} .

(vi) Mode VI: C/3

Phase I: (topology as “——” in Fig. 4(f))

S_i , S_1 , S_6 , S_9 , S_{10} turn on and S_o , S_2 - S_5 , S_7 , S_8 , S_{11} turn off. C_1 - C_3 are charged in series by the V_{pv} .

Phase II: (topology as “- - -” in Fig. 4(f))

S_o , S_1 , S_6 , S_9 , S_{10} turn on and S_i , S_2 - S_5 , S_7 , S_8 , S_{11} turn off. C_1 - C_3 are discharged in series to supply output capacitor C_o and battery load C_{bat} .

(vii) Mode VII: C/4

Phase I: (topology as “——” in Fig. 4(g))

S_i , S_1 , S_8 - S_{11} turn on and S_o , S_2 - S_7 turn off. C_1 - C_4 are charged in series by the V_{pv} .

Phase I: (topology as “- - -” in Fig. 4(g))

S_o , S_1 , S_8 - S_{11} turn on and S_i , S_2 - S_7 turn off. C_1 - C_4 are discharged in series to supply output capacitor C_o and battery load C_{bat} .

By changing the operation of the modes, the RSCC has the different circuit topologies so as to obtain the various equivalent resistance of the SC bank: $R_{eq}=1/(f_s \cdot mC)$, $m=4, 3, 2, 1, 1/2, 1/3, 1/4$. With regulating R_{eq} properly, we can perform the RSCC to track the MPP of PV module.

IV. OPERATION OF APO BASED CONTROLLER

Fig. 5 shows the flowchart of the APO algorithm. After power on initializations (block 1), input the I_{pv} and V_{pv} from PV module (block 2), then take the average of five point to calculate V_{pv1} , V_{pv2} , I_{pv1} and I_{pv2} (block 3). In block 4, compute the ΔV and ΔP . Then, according to ΔV and ΔP , the rules as below (block 5-11) will be performed for making a decision to increase or decrease the “running” number of buffer capacitors (denoted as: +C/-C):

If $\Delta P > 0$ and $\frac{\Delta P}{\Delta V} > 0$, then do -C; (-C \Rightarrow V_{pv} going up)

If $\Delta P > 0$ and $\frac{\Delta P}{\Delta V} < 0$, then do +C; (+C \Rightarrow V_{pv} going down)

If $\Delta P < 0$ and $\frac{\Delta P}{\Delta V} > 0$, then do +C; (+C \Rightarrow V_{pv} going down)

If $\Delta P < 0$ and $\frac{\Delta P}{\Delta V} < 0$, then do -C. (-C \Rightarrow V_{pv} going up)

Based on this APO algorithm, the equivalent capacitance can be regulated to change the up/down direction of the operating voltage V_{pv} so as to track the

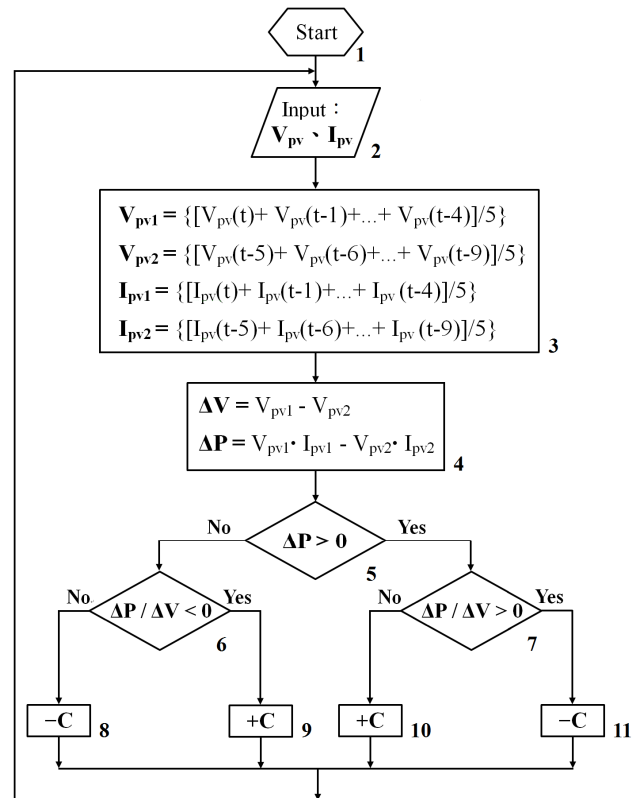


Fig. 5. Flowchart of the averaged P&O algorithm.

MPP of the PV module.

V. SIMULATION OF RSCC FOR MPPT

In this section, the proposed RSCC is designed and simulated by using OrCAD PSpice based on the scheme in Fig. 1. Here, a PV module contains 10 solar cells in series, and assume that the module has $V_{oc}=8.15V$ (open voltage) and $I_{rated}=100mA$ (rated current). In general, the solar voltage on MPP is about 70%~82% of V_{oc} , and the solar current on MPP is close to about 82~86% of I_{rated} [4]. Here, all components are listed as follows: $f_s=10$ kHz, $R_L=100\Omega$, $C_i=500\mu F$, $C=5\mu F$, $C_o=500\mu F$, $V_{bat}=1mF$, and the simulation cases include: (i) steady-state response, (ii) dynamic response to variation of I_{rated} .

(i) Steady-state response:

(a) CASE I: $I_{rated}=100mA$

Fig. 6(a) shows the steady-state waveforms of V_{pv-t} and P_{pv-t} . Obviously, the final value of P_{pv} is reaching about 610mW after 58ms. Fig. 6(b) shows the curves of $P_{pv}-V_{pv}$ and $I_{pv}-V_{pv}$, and it is found that the voltage on MPP is $V_{pv}=6.31V$ (about 78% of $V_{oc}=8.15V$) and MPP search can be achieved (MPP: $P_{pv,max}=610mW$).

(b) CASE II: $I_{rated}=150mA$

Fig. 7(a) shows the steady-state waveforms of V_{pv-t} and P_{pv-t} . Obviously, the final value of P_{pv} is reaching about 925mW after 34ms. Fig. 7(b) shows the curves of $P_{pv}-V_{pv}$ and $I_{pv}-V_{pv}$, and it is found that the voltage on MPP is $V_{pv}=6.61V$ (about 81% of $V_{oc}=8.15V$) and MPP search can be achieved (MPP: $P_{pv,max}=925mW$).

(c) CASE III: $I_{rated}=200mA$

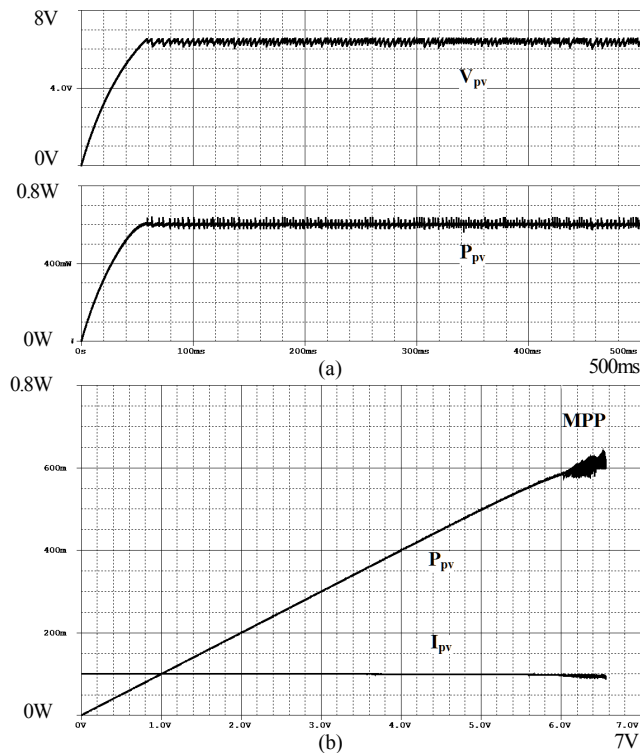


Fig. 6. Steady-state response as $I_{rated}=100mA$: (a) Waveforms of V_{pv} -t, P_{pv} -t, (b) Waveforms of P_{pv} - V_{pv} and I_{pv} - V_{pv} .

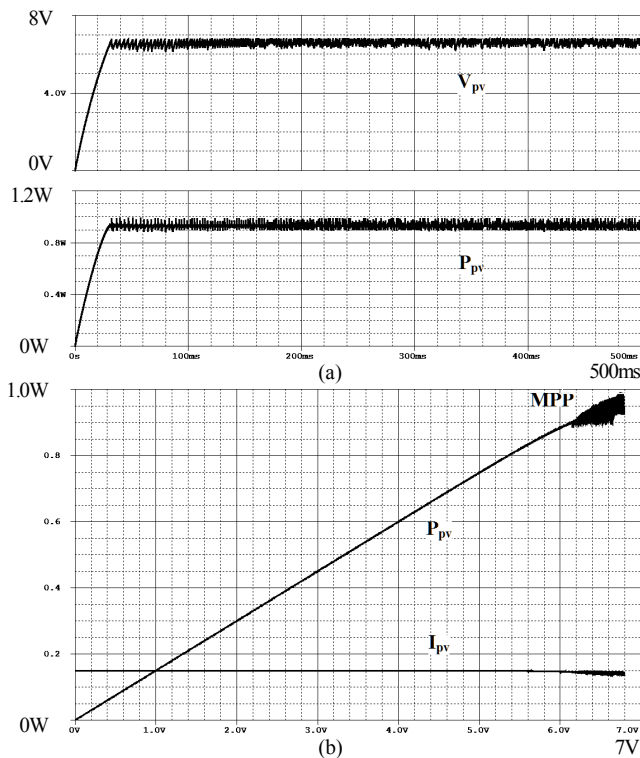


Fig. 7. Steady-state response as $I_{rated}=150mA$: (a) Waveforms of V_{pv} -t, P_{pv} -t, (b) Waveforms of P_{pv} - V_{pv} and I_{pv} - V_{pv} .

Fig. 8(a) shows the steady-state waveforms of V_{pv} -t and P_{pv} -t. Obviously, the final value of P_{pv} is reaching about 1.26W after 25ms. Fig. 8(b) shows the curves of P_{pv} - V_{pv} and I_{pv} - V_{pv} , and it is found that the voltage on MPP is $V_{pv}=6.72V$ (about 82% of $V_{oc}=8.15V$) and MPP search can be achieved (MPP: $P_{pv,max}=1.26W$).

Obviously, these results show that the RSCC has a

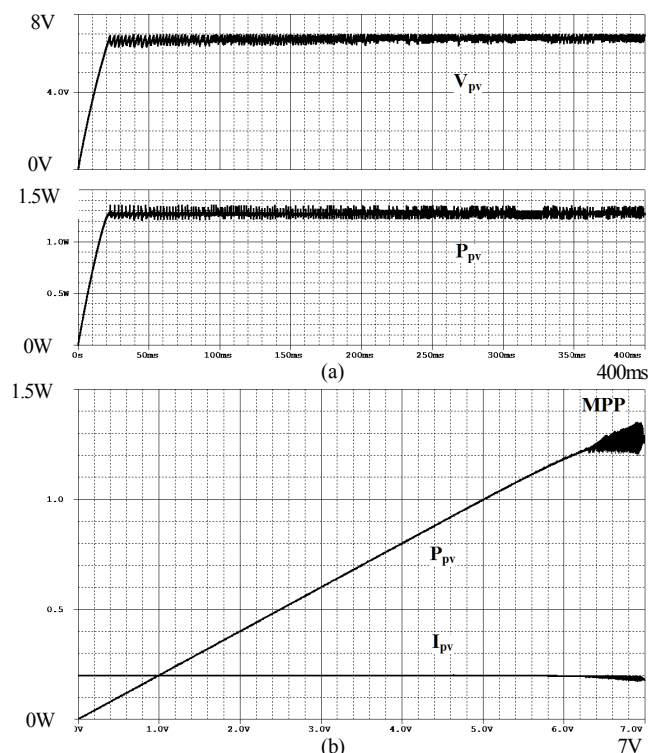


Fig. 8. Steady-state response as $I_{rated}=200mA$: (a) Waveforms of V_{pv} -t, P_{pv} -t, (b) Waveforms of P_{pv} - V_{pv} and I_{pv} - V_{pv} .

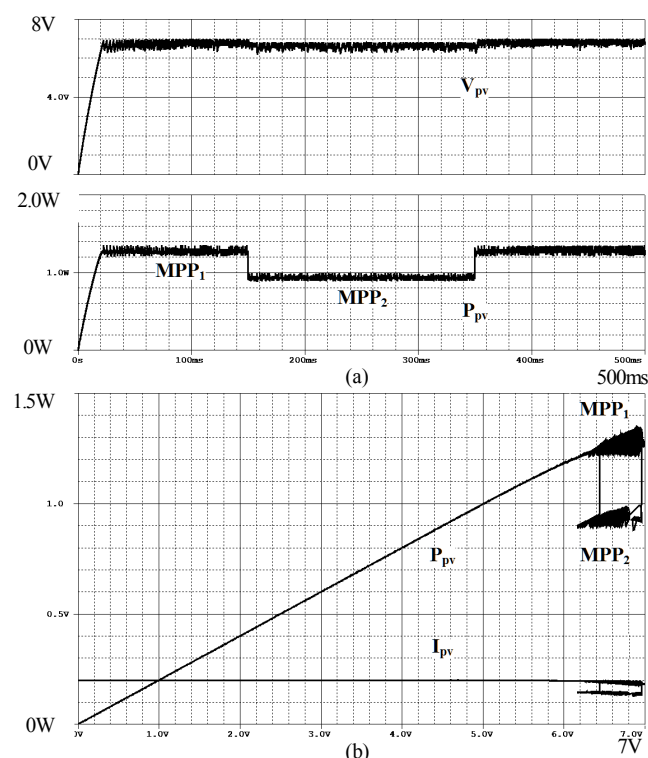


Fig. 9. Dynamic response as I_{rated} from 200mA \rightarrow 150mA: (a) Waveforms of V_{pv} -t, P_{pv} -t, (b) Waveforms of P_{pv} - V_{pv} and I_{pv} - V_{pv} .

pretty good steady-state performance.

(ii) Dynamic response

The dynamic response to the variation of I_{rated} (sunlight intensity changes suddenly) are discussed as follows.

(a) CASE I: $I_{rated}=200mA \rightarrow 150mA$

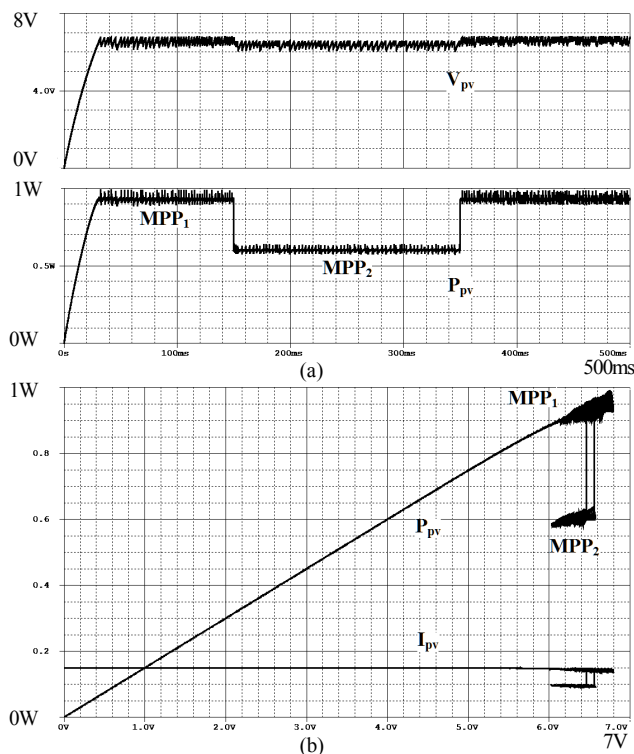


Fig. 10. Dynamic response as I_{rated} from 150mA→100mA: (a) Waveforms of V_{pv} -t, P_{pv} -t, (b) Waveforms of P_{pv} - V_{pv} and I_{pv} - V_{pv} .

Fig. 9(a) shows the dynamic waveforms of V_{pv} -t and P_{pv} -t. In the beginning, the value of P_{pv} is operating at MPP₁ (1.26W) when I_{rated} is 200mA, and then P_{pv} is quickly moving to the other MPP₂ (925mW) when I_{rated} is dropping to 150mA at 150ms. When I_{rated} recovers to 200mA, the operation of PV module gets back to MPP₁ from MPP₂ again. Fig. 9(b) shows the curves of P_{pv} - V_{pv} , and I_{pv} - V_{pv} , and it is found that the system is still keeping on the MPP₁ or MPP₂ at about 81%~82% of V_{oc} .

(b) CASE II: I_{rated} =150mA→100mA

Fig. 10(a) shows the dynamic waveforms of V_{pv} -t and P_{pv} -t. In the beginning, the value of P_{pv} is operating at MPP₁ (925mW) when I_{rated} is 150mA, and then P_{pv} is quickly moving to the other MPP₂ (610mW) when I_{rated} is dropping to 100mA at 150ms. When I_{rated} recovers to 150mA, the operation of PV module gets back to MPP₁ from MPP₂ again. Fig. 10(b) shows the curves of P_{pv} - V_{pv} , and I_{pv} - V_{pv} , and it is found that the system is still keeping on the MPP₁ or MPP₂ at about 78%~81% of V_{oc} .

Obviously, these results show that the APO-based RSCC has a pretty good dynamic performance.

VI. CONCLUSIONS

An APO-based RSCC is proposed for the MPPT of PV module system. The RSCC contains 7 modes to perform many different kinds of capacitance: 4C, 3C, 2C, C, C/2, C/3, and C/4. By using the APO algorithm, these 7 modes can be manipulated to increase or decrease the running number of buffer capacitors for the goal of MPPT. At present, we have been making the hardware prototype circuit of APO-based RSCC. Next, some more

experimental results will be measured for verification of this proposed scheme.

REFERENCES

- [1] N. V.Salas, E.Olías, A.Barrado, A. Lazaro, "Review of the maximum power point tracking algorithms for stand-alone photovoltaic systems," *Solar Energy Materials & Solar Cells.*, vol. 90, pp. 1555-1578, 2006.
- [2] N. Ozog, W. Xiao, and W. G. Dunford, "Topology study of photovoltaic interface for maximum power point tracking," *IEEE Trans. Ind. Electron.*, vol. 54, no. 3, pp. 1696-1704, Jun. 2007.
- [3] T. Tafticht, K. Agbossou, M.L. Doubia, A. Chériti "An improved maximum power point tracking method for photovoltaic systems," *Renewable Energy.*, vol. 33, issue 7, pp. 1508-1516, Jul. 2008.
- [4] H. L. Hey, J. D. P. Pacheco, J. Imhoff, and R. Gules, "A maximum power point tracking system with parallel connection for PV stand-alone applications," *IEEE Trans. Ind. Electron.*, vol. 55, no. 7, pp. 2674-2683, Jul. 2008.
- [5] J. K. Dickson, "On-chip high-voltage generation in MNOS integrated circuits using an improved voltage multiplier technique," *IEEE J. Solid-State Circuit.*, vol. SCC-11, no 2, pp. 374-378, Feb. 1976.
- [6] T. Tanzawa, and T. Tanaka, "A dynamic analysis of the Dickson charge pump circuit," *IEEE J. Solid-State Circuit.*, vol. 32, pp. 1231-1240, Aug. 1997.
- [7] S. V. Cheong, S. H. Chung, and A. Ioinovici, "Duty-cycle control boosts DC-DC converters," *IEEE Circuits and Devices Mag.*, vol 9, no. 2, pp. 36-37, 1993.
- [8] G. Zhu and A. Ioinovici, "Steady-state characteristics of switched-capacitor electronic converters," *J. Circuits, Syst. Comput.*, vol. 7, no. 2, pp. 69-91, 1997.
- [9] S. C. Tan, M. Nur, S. Kiratipongvoot, S. Bronstein, Y. M. Lai, C. K. Tse, and A. Ioinovici, "Switched-capacitor converter configuration with low EMI obtained by interleaving and its large-signal modeling" in *Proc. IEEE Int. Symp. Circuits Syst.* pp. 1081-1084, May 2009.
- [10] Y. H. Chang, "Variable conversion ratio multistage switched-capacitor voltage-multiplier/divider DC-DC converter," *IEEE Trans. Circuits Syst. I, Reg. Papers.*, vol. 58, no. 8, pp. 1944-1957, Aug. 2011.
- [11] Y. H. Chang, "Design and analysis of multistage multiphase switched-capacitor boost DC-AC inverter," *IEEE Trans. Circuits Syst. I, Reg. Papers.*, vol. 58, no. 1, pp. 205-218, Jan. 2011.
- [12] Y. H. Chang, and S. Y. Kuo, "A gain/efficiency-improved serial-parallel switched-capacitor step-up DC-DC converter," *IEEE Trans. Circuits Syst. I, Reg. Papers.*, vol. 60, no. 10, pp. 2799-2809, Oct. 2013.
- [13] Pradeep K. Peter and Vivek Agarwal, "On the input resistance of a reconfigurable switched-capacitor DC-DC converter-based maximum power point tracker of a photovoltaic source," *IEEE Trans. Power Electronics.*, vol. 27, no. 12, pp. 4880-4893, Dec. 2012.